

# Unequal Teeth Design to Reduce Electromagnetic Vibration in Fractional-Slot Concentrated-Windings Permanent-Magnet Machine

Shengdao Zhu, Jinghua Ji\*, Wenxiang Zhao, Junqiang Zheng, Yanxin Mao, and Guohai Liu

*School of Electrical and Information Engineering, Jiangsu University, Zhenjiang 212013, China*

(Received 9 November 2018, Received in final form 28 October 2019, Accepted 28 October 2019)

**This paper presents a new stator topology of fractional-slot concentrated-windings permanent-magnet (FSCW-PM) machine in order to reduce the electromagnetic vibration. First of all, the space orders and corresponding frequencies of the lowest order radial force of FSCW-PM machines is studied. A 12-slot/10-pole FSCW-PM machine is used as an example, and its lowest order radial force harmonics are calculated by analytical method and finite element method, respectively. Then, in order to minimize the amplitude of the vibration acceleration, a new stator structure of 12-slot/10-pole machine is designed, by which the amplitude of the lowest order radial force is greatly reduced. Afterwards, the modal and vibration experiments are performed. The result shows that the 2<sup>nd</sup> order radial force with  $2f_0$  frequency contributes most to overall vibration. Finally, vibration simulation models of both machines are established, the results show that the machine with unequal teeth design effectively reduce the electromagnetic vibration.**

**Keywords :** fractional-slot concentrated-windings (FSCWs), permanent-magnet machines, radial force, modal analysis, electromagnetic vibration

## 1. Introduction

Fractional-slot concentrated-windings permanent-magnet (FSCW-PM) machines have received great attention in many fields due to their advantages such as easy manufacture, high power density, high efficiency, low torque ripple, good flux-weakening and fault-tolerant performance [1-3]. However, the abundant armature magnetomotive force (MMF) harmonics in FSCW-PM machines produce low-order radial force harmonics, which aggravating the electromagnetic vibration performance [4, 5]. Especially in low-vibration applications such as household appliances, electric vehicles and naval vessels [6-8], low electromagnetic vibration is a critical indicator to electric machines.

Differing from integer-slot PM machines, FSCW-PM machines suffer from high electromagnetic vibration. This is because the existence of low-order radial force harmonics. Refs. [9-11] investigated the electromagnetic performance and vibration characteristics of FSCW-PM machines, which have different slot ( $Q_s$ ) and pole ( $2p$ ) combinations. For the selections of slot and pole combination, it is

difficult for a machine to acquire both high torque density and low electromagnetic vibration at the same time. The high least common multiple (LCM) of slots and poles is required to increase windings factor while high greatest common divisor (GCD) of slots and poles is required to restrain low-order radial force harmonics. The most popular selections of the FSCW-PM machine topologies in electric machine include 9-slot/6-pole, 12-slot/8-pole, 12-slot/10-pole and 15-slot/10-pole, among which the 12-slot/10-pole one has the greatest LCM ( $Q_s, 2p$ ) and the least GCD ( $Q_s, 2p$ ). Hence, the 12-slot/10-pole FSCW-PM machine possesses the highest windings factor and torque density. Regrettably, this machine suffers from significant 2<sup>nd</sup> order radial force which can cause excessive vibration in the machine.

It is well known that the radial force results from the interaction between PM field and armature reaction field harmonics. Recently, many techniques have been reported to decrease or even eliminate some specific armature MMF harmonics, adopting delta-star windings, using asymmetric number of turns and applying phase shift by doubling slot numbers were studied in [12-14]. However, these MMF harmonics reduction methods are effectual to specific harmonics but immune to the tooth harmonics. Also, it has been revealed in [15] that the elimination of sub-

©The Korean Magnetism Society. All rights reserved.

\*Corresponding author: Tel: +86-511-88722598

Fax: +86-511-88722598, e-mail: jjh@ujs.edu.cn

harmonics have little impact on reducing electromagnetic vibration.

Moreover, in order to reduce low-order radial force and electromagnetic vibration, several optimal methods on geometry of FCSW-PM machines have been proposed. Ref. [16] proposed three novel stator structures based on inserting auxiliary slots, and these methods have different effect on reducing unbalanced magnetic force. In [17], the proposed FT-FSPM machines with skew rotor teeth and double fault tolerant teeth provide desirable reduction of electromagnetic vibration and noise. Besides, the relationship between radial force and slot opening width is studied to reduce the electromagnetic vibration and noise [18]. The result shows that the optimized machine has decreased electromagnetic noise up to 6dB than the original one. However, the aforementioned methods suffer from torque sacrifice, and they are restricted by the machine operation modes. Ref. [19] proposes a new method to reduce the tooth harmonics in FSCW-PM machine. The paper with unequal tooth design only mentions that this technique is beneficial for reducing motor vibration. However, it lacks further explanation and analyses of the specific reasons for motor vibration reduction.

This paper aims to reduce the electromagnetic vibration of the FSCW-PM machine with unequal tooth techniques, and it contains electromagnetic analysis, structural modal analysis and vibration response analysis. First of all, the expression of space order and corresponding frequency of radial force for FSCW-PM machines is derived. Also, the lowest order radial force harmonics are analytical calculated, and it verified by finite element method (FEM). According to the MMF harmonics source of the lowest order radial force, a new stator structure of 12-slot/10-pole FSCW-PM machine is designed to reduce the lowest order radial force harmonic and electromagnetic vibration. It is pointed out that the output torque capability of the newly designed machine can be kept same as the original one. Then, vibration modes and corresponding natural frequencies are predicted by FEM, and the vibration analysis is performed to predict vibration acceleration by modal superposition method. Finally, the effect of vibration reduction of the designed machine is validated by simulated results. Also, the predicted vibration acceleration results show that the newly designed machine effectively reduces the electromagnetic vibration.

## 2. Radial Force Analysis

The amplitude of vibration displacement is approxi-

mately inversely proportional to the fourth power of the radial force order. Hence, the lowest order of radial force plays a dominant role in generating electromagnetic vibration [20]. In order to reduce the lowest order radial force, it is necessary to investigate the generation principle of the lowest order radial force.

According to Maxwell Stress Tensor method, the radial force  $P_r(\theta, t)$  can be expressed as [21]

$$P_r(\theta, t) = \frac{B_r^2(\theta, t) - B_t^2(\theta, t)}{2\mu_0} \approx \frac{B_r^2(\theta, t)}{2\mu_0} \quad (1)$$

where  $B_r(\theta, t)$  and  $B_t(\theta, t)$  are radial and tangential flux density in air-gap, respectively,  $\mu_0$  is the permeability of vacuum,  $t$  is the time and  $\theta$  is the space mechanical angle. The tangential flux density can be neglected because of its insignificant amplitude.

Considering the stator slotting effect in FSCW-PM machine, the air-gap permeability is no longer a constant. Air-gap permeance distribution function  $\lambda_{gap}$  can be expressed as

$$\lambda_{gap} = \lambda_0 + \sum_k \lambda_k \cos(kQ_s\theta) \quad (2)$$

where  $\lambda_0$  is the average air-gap permeance,  $k$  is the order of permeance,  $\lambda_k$  is the amplitude of  $k^{\text{th}}$  permeance. The radial force generated by the interaction between the PM magnetic field flux density and armature reaction flux density. The PM magnetic field flux density  $B_{pm}$  can be expressed as

$$\begin{aligned} B_{pm} &= F_{pm} \cdot \lambda_{gap} \\ &= \sum_{v_r} F_r \cos v_r(p\theta - \omega t) \cdot [\lambda_0 + \sum_k \lambda_k \cos(kQ_s\theta)] \\ &= \sum_{v_r} F_r \cdot \lambda_0 \cos v_r(p\theta - \omega t) + \sum_k \sum_{v_r} \frac{F_r \cdot \lambda_k}{2} \\ &\quad \cos[(v_r p + kQ_s)\theta - v_r \omega t] \\ &\quad + \sum_k \sum_{v_r} \frac{F_r \cdot \lambda_k}{2} \cos[(v_r p - kQ_s)\theta - v_r \omega t] \\ &= \sum_{v_r} B_r \cos v_r(p\theta - \omega t) + \sum_k \sum_{v_r} B_{rk} \cos[(v_r p + kQ_s)\theta - v_r \omega t] \\ &\quad + \sum_k \sum_{v_r} B_{rk} \cos[(v_r p - kQ_s)\theta - v_r \omega t] \end{aligned} \quad (3)$$

where  $F_{pm}$  is the MMF of PM magnetic field,  $v_r$  is the order of PM MMF harmonics,  $F_r$  and  $B_r$  are the amplitude of  $v_r^{\text{th}}$  PM magnetic field MMF and flux density,  $\omega$  is the electromagnetic angular velocity. Also, the armature reaction flux density  $B_{arm}$  can be expressed as

$$\begin{aligned}
B_{arm} &= F_{arm} \cdot \lambda_{gap} \\
&= \sum_{v_s} F_s \cos(v_s \theta - \mu \omega t) \cdot [\lambda_0 + \sum_k \lambda_k \cos(k Q_s \theta)] \\
&= \sum_{v_s} F_s \cdot \lambda_0 \cos(v_s \theta - \mu \omega t) + \sum_k \sum_{v_s} \frac{F_s \cdot \lambda_k}{2} \\
&\quad \cos[(v_s + k Q_s) \theta - \mu \omega t] \\
&+ \sum_k \sum_{v_s} \frac{F_s \cdot \lambda_k}{2} \cos[(v_s - k Q_s) \theta - \mu \omega t] \quad (4) \\
&= \sum_{v_s} B_s \cos(v_s \theta - \mu \omega t) + \sum_k \sum_{v_s} B_{sk} \cos[(v_s + k Q_s) \theta - \mu \omega t] \\
&+ \sum_k \sum_{v_s} B_{sk} \cos[(v_s - k Q_s) \theta - \mu \omega t]
\end{aligned}$$

where  $F_{arm}$  is the PM MMF,  $v_s$  is the order of armature reaction MMF harmonics,  $F_s$  and  $B_s$  are the amplitude of  $v_s^{\text{th}}$  armature reaction magnetic field MMF and flux density,  $\mu$  is the rotation direction of the  $v_s^{\text{th}}$  armature reaction MMF harmonic, with -1 for forward rotating and 1 for backward rotating. The air-gap radial flux density  $B_r(\theta, t)$  contains two parts, when the saturation of the magnetic field is ignored. It can be written as

$$B_r(\theta, t) = B_{pm}(\theta, t) + B_{arm}(\theta, t) \quad (5)$$

Substituting (3)-(5) into (1), the radial force can be expressed as

$$\begin{aligned}
P_r(\theta, t) &\approx \frac{B_r^2(\theta, t)}{2\mu_0} \\
&= \frac{1}{2\mu_0} (B_{pm}^2(\theta, t) + B_{arm}^2(\theta, t) + 2B_{pm}(\theta, t)B_{arm}(\theta, t)) \\
&= \frac{1}{2\mu_0} \left\{ \sum_{v_r} B_r \cos v_r (p\theta - \omega t) \right. \\
&\quad + \sum_{v_r} \sum_k B_{rk} \cos[(v_r p + k Q_s) \theta - v_r \omega t] \\
&\quad + \left. \sum_{v_r} \sum_k B_{rk} \cos[(v_r p - k Q_s) \theta - v_r \omega t] \right\}^2 \\
&+ \frac{1}{2\mu_0} \left\{ \sum_{v_s} B_s \cos(v_s \theta - \mu \omega t) \right. \\
&\quad + \sum_k \sum_{v_s} B_{sk} \cos[(v_s + k Q_s) \theta - \mu \omega t] \\
&\quad + \left. \sum_k \sum_{v_s} B_{sk} \cos[(v_s - k Q_s) \theta - \mu \omega t] \right\}^2 \quad (6) \\
&+ \frac{1}{\mu_0} \left\{ \sum_{v_r} B_r \cos v_r (p\theta - \omega t) \right. \\
&\quad + \sum_{v_r} \sum_k B_{rk} \cos[(v_r p + k Q_s) \theta - v_r \omega t] \\
&\quad + \sum_{v_r} \sum_k B_{rk} \cos[(v_r p - k Q_s) \theta - v_r \omega t] \\
&\quad \cdot \left. \sum_{v_s} B_s \cos(v_s \theta - \mu \omega t) \right. \\
&\quad + \sum_k \sum_{v_s} B_{sk} \cos[(v_s + k Q_s) \theta - \mu \omega t] \\
&\quad + \left. \sum_k \sum_{v_s} B_{sk} \cos[(v_s - k Q_s) \theta - \mu \omega t] \right\}
\end{aligned}$$

**Table 1.** Space order and corresponding frequency of radial force harmonics.

Category	Space order	frequency
$B_{pm}^2$	$(v_{r1} \pm v_{r2})p$	$(v_{r1} \pm v_{r2})f_0$
	$(v_{r1} \pm v_{r2})p \pm 2Q_s$	$(v_{r1} \pm v_{r2})f_0$
	$(v_{r1} \pm v_{r2})p \pm Q_s$	$(v_{r1} \pm v_{r2})f_0$
$B_{arm}^2$	$(v_{s1} \pm v_{s2})p$	$2f_0/0$
	$(v_{s1} \pm v_{s2})p \pm 2Q_s$	$2f_0/0$
	$(v_{s1} \pm v_{s2})p \pm Q_s$	$2f_0/0$
$2B_{pm}B_{arm}$	$(v_r \pm v_s)p$	$(v_r \pm 1)f_0$
	$(v_r \pm v_s)p \pm Q_s$	$(v_r \pm 1)f_0$
	$(v_r \pm v_s)p \pm 2Q_s$	$(v_r \pm 1)f_0$

According to the magnetic harmonic sources, the radial force can be divided into three categories, namely  $B_{pm}^2$ ,  $B_{arm}^2$  and  $2B_{pm}B_{arm}$ , and each category can be divided into three parts after polynomial expansion. To simplify calculations, only the 1<sup>st</sup> tooth permeance is considered, and the space orders with corresponding frequencies of nine parts are summarized in Table 1, where  $f_0$  is the electric frequency of machine.

It can be seen that low-order radial force harmonics are caused by the air-gap magnetic field and stator slotting effect. It is worth noting that the lowest order of radial force for FSCW-PM machines with close number of slots and poles is  $Q_s - 2p$ . Actually, the value of  $Q_s - 2p$  is always equal to that of  $GCD(Q_s, 2p)$ , so the FSCW-PM machines with close number of slots and poles, such as 9-slot/8-pole, 12-slot/10-pole and 15-slot/14-pole have worse vibration performance.

### 3. Validation of Radial Force Derivation

As shown in Fig. 1, in order to verify the above-mentioned derivation of the radial force, a 12-slot/10-pole FSCW-PM machine is used to verify its correctness. This machine has excellent electromagnetic characteristics such as low torque pulsation, high efficiency and good fault tolerance. However, it is unsuitable for the low vibration applications due to the large amplitude of 2<sup>nd</sup> order radial force harmonics. In this Section, the lowest order of radial force components are calculated by analytical method, and above derivation of radial force orders and frequencies distribution are verified by 2-D fast Fourier transform. Main parameters of the 12-slot/10-pole FSCW-PM machine are listed in Table 2.

As mentioned above, FSCW-PM machines suffer from

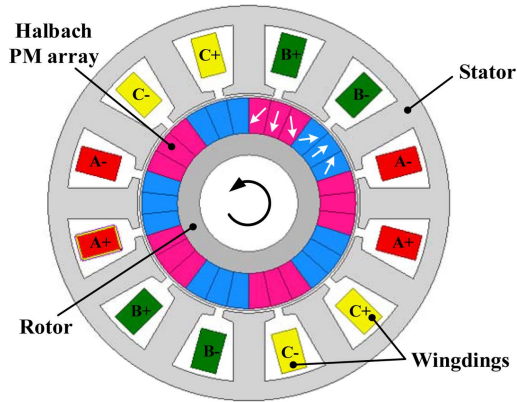


**Fig. 1.** (Color online) Cross section of 12-slot/10-pole FSCW-PM machine.

**Table 2.** Main parameters of the FSCW-PM machine.

Parameters	Unit	Value
Number of poles and slots	-	10p12s
GCD(slots, poles)	-	2
Rotation speed	r/min	1000
Stator outer diameter	mm	90
Stator inner diameter	mm	55
Stator yoke thickness	mm	4.7
Stacking length	mm	120
Length of air-gap	mm	1
Peak phase current	A	15
Turns per slot	-	33
Current frequency	Hz	83.3
Remanence of PM	T	1.09
Stator lamination	-	B20AT1500

abundant armature magnetic field harmonics, and these harmonics will interact with PM field harmonics to produce low-order radial force harmonics. PM flux density harmonics and armature flux density harmonics are shown in Fig. 2.

The 2<sup>nd</sup> order radial force is mainly produced by flux density harmonics with order difference of 2, such as 5<sup>th</sup> PM field and 7<sup>th</sup> armature field, 5<sup>th</sup> armature field and 7<sup>th</sup> armature field, 11<sup>th</sup> armature field and 13<sup>th</sup> armature field. Table 3 lists the amplitude and frequency of each 2<sup>nd</sup> order radial force harmonics resulted from different flux density harmonics. Since the 5<sup>th</sup> PM field has the largest amplitude, the interaction between 5<sup>th</sup> PM field and 7<sup>th</sup> armature field is the dominant component of 2<sup>nd</sup> order radial force. It worth noted that the same order compo-

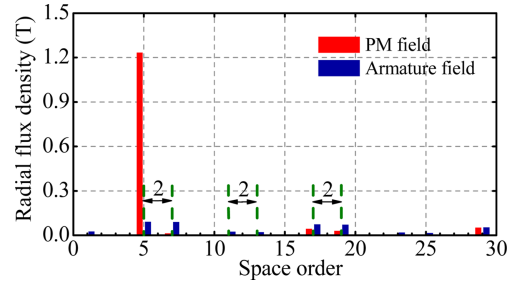


**Fig. 2.** (Color online) Radial flux density of PM and armature field.

**Table 3.** Calculation of 2<sup>nd</sup> radial force harmonics.

Harmonics	Vector(N/cm <sup>2</sup> )	Amp(N/cm <sup>2</sup> )	Freq(Hz)
( $v_r=5, v_s=7$ )	0.4622+0.0099i	0.4623	$2f_0$
( $v_r=5, v_s=7$ )	<b>-0.1436+3.9322i</b>	<b>3.9334</b>	<b><math>2f_0</math></b>
( $v_r=7, v_s=5$ )	0.0007-0.0340i	0.0341	$2f_0$
( $v_r=11, v_s=13$ )	-0.0036-0.0005i	0.0036	$2f_0$
( $v_r=17, v_s=19$ )	0.0009-0.0062i	0.0063	$2f_0$
Total	0.1665+7.6022i	3.7826	-

nent of radial force should be superposed by vectors, rather than amplitude, hence some radial force harmonics may even decrease the total amplitude.

Radial force is a function of time and space, and 2-D fast Fourier transform is conducted to obtain the order and frequency of each radial force harmonics. Fig. 3 shows the 2-D Fourier decomposition of the radial force at current 15 A and 1000 r/min. The 2<sup>nd</sup> order radial force with  $2f_0$  frequency is marked by green circles. Although the amplitude of 2<sup>nd</sup> radial force is relatively small, it can excite large electromagnetic vibration due to its lower order. The 10<sup>th</sup> radial force has the greatest amplitude, but the impact on electromagnetic vibration is not obvious due to its higher order. Therefore, without sacrificing the

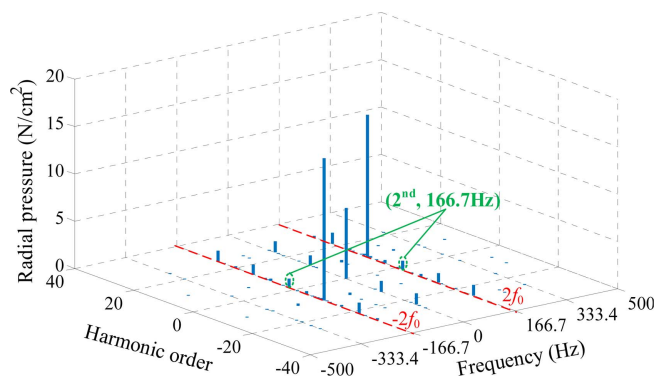


**Fig. 3.** (Color online) Space and time decomposition of radial pressure.

output torque, reducing the lowest order radial force harmonic is the most effective method to suppress the electromagnetic vibration.

### 4. New Stator Design

The 2<sup>nd</sup> order radial force is the main reason for over-large electromagnetic vibration in the 12-slot/10-pole machine. It can be seen from Table 3 that the 2<sup>nd</sup> order radial force mainly resulted from the interaction between 5<sup>th</sup> order PM field and 7<sup>th</sup> order armature field harmonic. The 5<sup>th</sup> order PM field is the working wave, which relates to the output torque. So, reducing the 7<sup>th</sup> order armature field harmonic is the key point to decrease the 2<sup>nd</sup> order radial force.

As can be seen from (4), in addition to the  $p^{\text{th}}$  order flux density, it also exhibits  $(p+Q_s)^{\text{th}}$  and  $(p-Q_s)^{\text{th}}$  order flux density harmonics. These specific harmonics are the so-called tooth harmonics which caused by stator slotting. In FSCW-PM machines, these specific armature MMF harmonics order are satisfied

$$v_s = |kQ_s \pm p| \tag{7}$$

Because the tooth harmonics have same winding factors with that of the fundamental wave, conventional MMF harmonics reduction methods are immune to them. Fig. 4 shows the newly designed stator structure of a 12-slot/10-pole FSCW-PM machine with unequal teeth, as compared with the existing one. In addition to the slot opening position, the newly designed machine has the same parameters with that of the existing one, as listed in Table 2. Since the magnetic field always takes the path with the smallest reluctance. The magnetic field flux line distribution of the proposed machine has changed due to the offset of slots position. The magnetic field flux line distribution of the proposed design and existing machine are shown in Fig. 5.

It is well known that the magnitude of each order

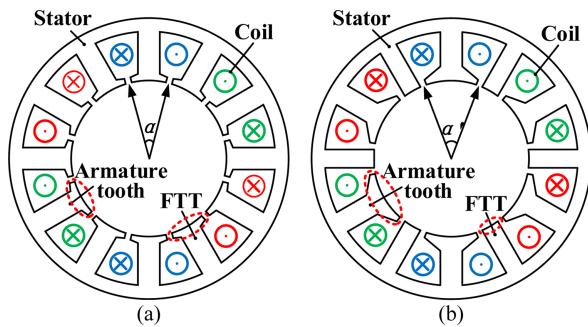


Fig. 4. (Color online) Stator structures of both 12-slot/10-pole machines. (a) Existing. (b) Proposed.

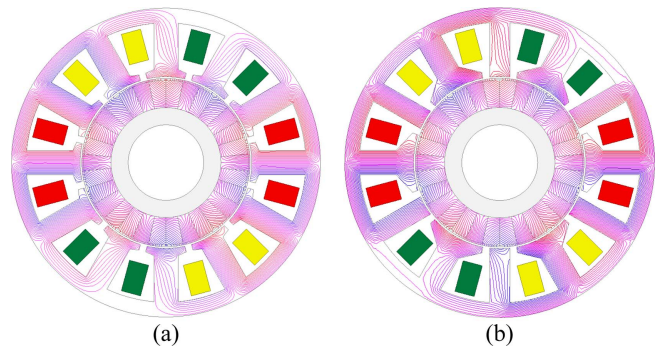


Fig. 5. (Color online) Magnetic field flux line distribution. (a) Existing. (b) Proposed.

armature MMF can be expressed as

$$F_s = \frac{m\sqrt{2}}{\pi v_s} N k_N I \tag{8}$$

where  $m$  is the phase number,  $N$  is the total number of turns in one phase,  $I$  is the magnitude of current,  $k_N$  is the windings factor, and  $k_N$  can be expressed as

$$\begin{cases} k_N = k_q \cdot k_y \\ k_q = \cos \frac{\alpha}{2} \\ k_y = \sin \left( \frac{v_s \alpha}{2} \right) \end{cases} \tag{9}$$

where  $k_q$  and  $k_y$  are distribution factor and pitch factor,  $\alpha$  is adjacent slot opening angle. Therefore, the relationship between the magnitude of each armature MMF harmonics, harmonic order  $v_s$  and adjacent slot opening angle  $\alpha$  can be expressed as

$$F_s \propto \frac{\sin(v_s \cdot \frac{\alpha}{2})}{v_s} \tag{10}$$

As shown in Fig. 6, the amplitude of 1<sup>st</sup>, 5<sup>th</sup> and 7<sup>th</sup> order armature MMF harmonics vary with the adjacent slot opening angle  $\alpha$ . In order to keep the 5<sup>th</sup> order MMF

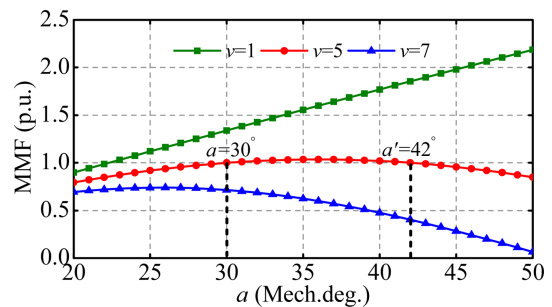
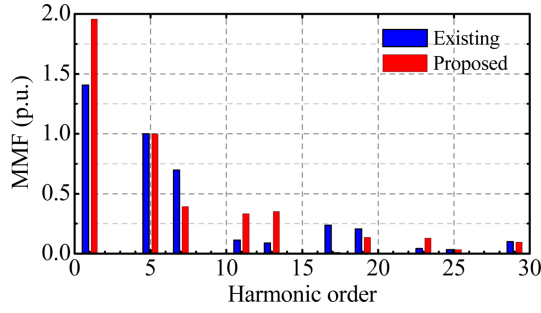
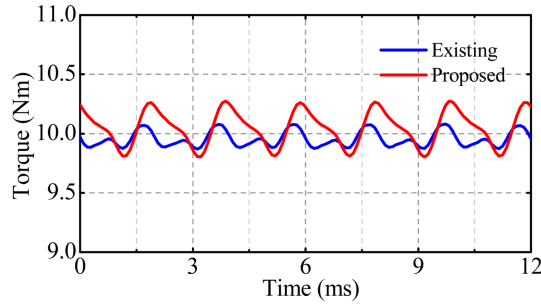


Fig. 6. (Color online) Armature MMF variation.



**Fig. 7.** (Color online) MMF comparison spectrum of both machines.



**Fig. 8.** (Color online) Output torque comparison of both machines.

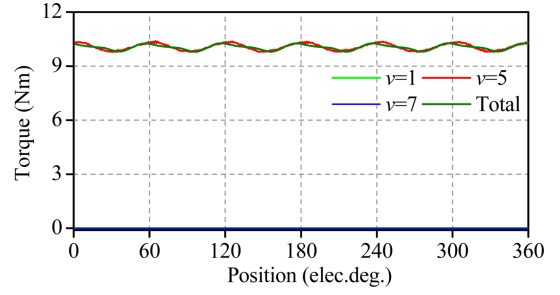
harmonic constant,  $\alpha = 42$  mechanical degree has been selected as shown in Fig. 4. Under this circumstance, the 7<sup>th</sup> order MMF tooth harmonic is significantly reduced in the proposed machine. Each MMF space harmonics are shown in Fig. 7. Although some MMF harmonics such as 1<sup>st</sup>, 11<sup>th</sup> and 13<sup>th</sup> order have increased, their contributions to the 2<sup>nd</sup> order radial force are extremely weak.

Fig. 8 shows the electromagnetic output torque. Since the 5<sup>th</sup> order working wave keeps unchanged, the average output torque of the designed machine is almost unchanged. The Maxwell stress method can be used for calculating the motor electromagnetic torque, and the electromagnetic torque can be expressed as

$$T_e(t) = \frac{R^2 l_{ef}}{\mu_0} \int_0^{2\pi} B_r B_t d\theta = \sum_v T_v(t) \quad (11)$$

where  $R$  is the radius of the air-gap,  $l_{ef}$  is the laminated length,  $m_0$  is the vacuum permeability,  $B_r$  and  $B_t$  are the radial and tangential components of the flux density under rate load,  $T_v$  is the electromagnetic torque generated by the  $v^{\text{th}}$  order flux density harmonic.  $B_r$ ,  $B_t$  and  $T_v$  can be expressed as

$$\begin{cases} B_r(t, \theta) = \sum_v B_{rv} \cos[v\theta - \theta_{rv}(t)] \\ B_t(t, \theta) = \sum_v B_{tv} \cos[v\theta - \theta_{tv}(t)] \end{cases} \quad (12)$$



**Fig. 9.** (Color online) Contribution of different flux density harmonics to electromagnetic torque.

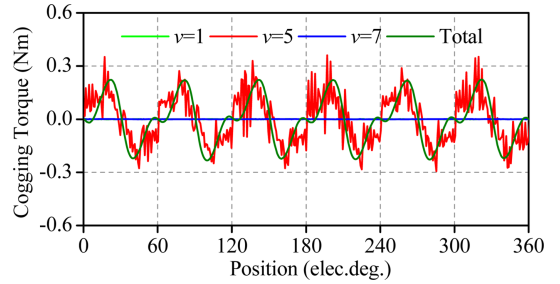


**Fig. 10.** (Color online) Contribution of different flux density harmonics to cogging torque.

$$T_v(t) = \frac{\pi R^2 l_{ef}}{\mu_0} B_{rv} B_{tv} \cos[\theta_{rv}(t) - \theta_{tv}(t)] \quad (13)$$

where  $B_{rv}$  and  $B_{tv}$  are the amplitude of  $v^{\text{th}}$  order radial and tangential flux density harmonics.  $q_{rv}$  and  $q_{tv}$  are the phase of  $v^{\text{th}}$  order radial and tangential flux density harmonics. From (12) and (13), it can be concluded that only the same harmonic order of flux density harmonics can produce a stable electromagnetic torque. Fig. 9 shows the contribution of 1<sup>st</sup>, 5<sup>th</sup> and 7<sup>th</sup> order flux density harmonics to electromagnetic torque. It can be seen that the 1<sup>st</sup> and 7<sup>th</sup> order flux density harmonics have little contribution to the electromagnetic torque, and the total torque of the machine is mainly generated by the 5<sup>th</sup> flux density harmonic.

The proposed machine has larger torque ripple than the existing one, and the main reason is that the cogging torque of the proposed machine has increased. The cogging torque can be calculated by using the Maxwell stress method. The contribution of different flux density harmonics to cogging torque is shown in Fig. 10. It can be seen that the maximum contribution to the cogging torque is the 5<sup>th</sup> order flux density harmonic, and the 1<sup>st</sup> and 7<sup>th</sup> order flux density harmonics have little effect on the cogging torque. Due to the slot position offset of the proposed machine, the 6<sup>th</sup> order cogging torque harmonic component cannot be cancelled out. Therefore, the offset of the slots position is responsible for the increased cogging torque of the proposed machine, rather than the changes of the flux

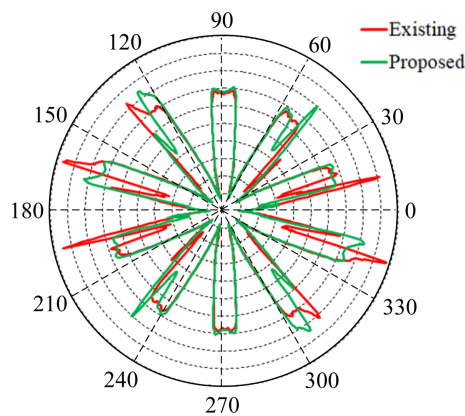


Fig. 11. (Color online) Spatial distribution of radial force.

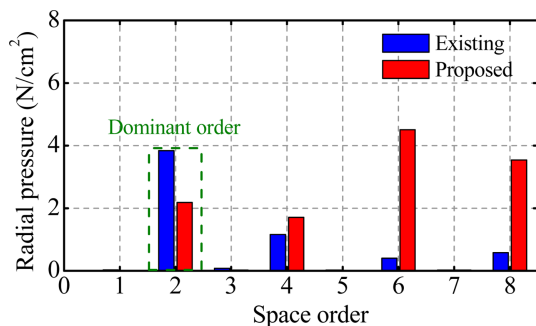


Fig. 12. (Color online) Radial force spectrum comparison of both machines.

density harmonics.

Fig. 11 is the spatial distribution of radial force at a certain moment. It can be clearly seen that the newly designed machine has more uniform spatial distribution of radial force than the existing one. It can be concluded that the existing machine contains more 2<sup>nd</sup> order radial force components. Spatial spectrum analysis of radial force is performed to obtain the accurate content of each order radial force, and the first 8 orders of radial force are shown in Fig. 12. Compared with that of the existing FSCW-PM machine, the 2<sup>nd</sup> order radial force of the proposed one is reduced about 43.2 %. It is mainly because the newly designed stator structure can effectively reduce the 7<sup>th</sup> order MMF tooth harmonic. In addition, the increase of the 4<sup>th</sup>, 6<sup>th</sup> and 8<sup>th</sup> order harmonics have little influence on electromagnetic vibration for their high order.

## 5. Electromagnetic Vibration Analysis

### 5.1. Modal analysis

The radial force has been calculated by Maxwell Stress Tensor method, which will be applied as an excitation on the stator inner surface, thus causing electromagnetic vibration. Through the modal analysis, the natural frequency,

damping and modal shape characteristics of the structure can be obtained. Actually, vibration response is the superposition of various vibration modes. In order to study the dynamic characteristics of the machine structure, the basic dynamic equation for the machine is built and expressed as

$$[M]\{\ddot{x}(t)\} + [C]\{\dot{x}(t)\} + [K]\{x(t)\} = \{F(t)\} \quad (14)$$

where  $[M]$ ,  $[C]$ , and  $[K]$  are the mass, damping, and stiffness matrices, respectively,  $\{x(t)\}$  is the vibration displacement vector, and  $\{F(t)\}$  is the excitation.

Generally, the damping of machine stator can be neglected because it is quite small. When the excitation  $\{F(t)\}$  is not applied and the damping is neglected, (14) can be derived as

$$[M]\{\ddot{x}(t)\} + [K]\{x(t)\} = 0 \quad (15)$$

Therefore, the modal frequency can be written as

$$f_n = \frac{1}{2\pi} \sqrt{\frac{K}{M}} \quad (16)$$

Modal frequency is subject to the distribution of stiffness and mass. Namely, the modal frequency can be adjusted by modifying the structure parameters to avoid machine resonance.

A 3-D structural model is established to obtain modal parameters. Since the stiffness of the winding can be ignored, the winding can be equivalent to the mass and

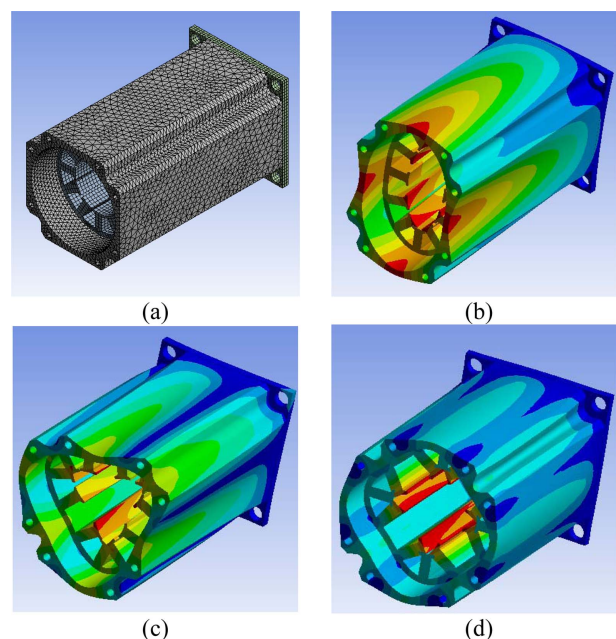


Fig. 13. (Color online) FEM model and mode shapes. (a) Mesh. (b) 2nd mode (2125 Hz). (c) 3rd mode (5080 Hz). (d) 4th mode (7489 Hz).

attached to the stator teeth. Fig. 13 shows the mesh of 3-D FEM model and the first 4 order modes. Since the housing and end cap increase structural stiffness of the stator assembly, these modal frequencies are much higher than that of radial force. The first 4 orders of modal frequencies are 2125 Hz, 5080 Hz, and 7489 Hz. For the 12-slot/10-pole machine. Since the 2<sup>nd</sup> order radial force harmonics and the 2<sup>nd</sup> order mode play dominant roles in generating vibration, the modal experiment will be conducted to further study the vibration characteristics in the next section.

**5.2. Vibration analysis**

When the machine rotates, the alternating radial force will produce electromagnetic vibration displacement on the stator. The forced vibration displacement amplitude  $Y_n$  is expressed as

$$Y_n = \frac{P_r(\theta_s, t)}{K - \omega_r^2 M} = \frac{R^3 F_r(\theta_s, t)}{2\pi F_n^2 E J (n^2 - 1)^2 \left[ 1 - \left( \frac{f_r}{f_n} \right)^2 \right]} \quad (17)$$

where  $\omega_r$  is angular frequency of radial electromagnetic force,  $R$  is average radius of stator yoke,  $E$  is the elastic modulus,  $J$  is structural geometry parameter,  $n$  represents the radial force order, and  $f_r$  is the radial force frequency. In order to verify the electromagnetic vibration of both 12-slot/10-pole machines, 2-D electromagnetic and 3-D structural model are established. Fig. 14 shows the predicted vibration acceleration spectrogram of the 12-slot/10-pole machine. It can be seen that the largest value of the vibration acceleration is about 1.6 m/s<sup>2</sup>, and it occurred at 167 Hz, the frequency of the maximum value matches well with that of the 2<sup>nd</sup> order radial force. In addition, the peak values of vibration acceleration appear at an even multiple of the electrical frequency, and the vibration acceleration at 2<sup>nd</sup> modal frequency is relatively large.

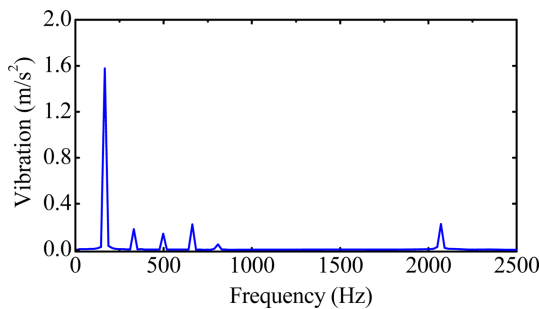


**Fig. 14.** (Color online) Predicted electromagnetic vibration acceleration spectrogram.

**6. Experiment Validation**

**6.1. Modal Experiment**

Modal experiment is conducted to obtain actual modal parameters and compare with the FEM modal simulation. As shown in Fig. 15, the stator assembly is suspended in a free state. The predicted and measured vibration shapes and frequencies of 2<sup>nd</sup> order vibration mode are compared in Table 4. The error between FEM-predicted and measured results is about 0.8 %, so the 3-D structure FEM results is accurate. Since the existing and newly designed stator structures are similar in geometric parameters, their modal shapes and corresponding natural frequencies are almost same. So, the modal analysis is conducted only for the existing stator to avoid repeated operations. For both 12-slot/10-pole machines, the 2<sup>nd</sup> order radial force frequency is 167 Hz, which is far from the 2<sup>nd</sup> order modal frequency of 2125 Hz, the resonance will not happen for such huge difference.

**6.2. Vibration Experiment**

Fig. 16 shows the prototype of the 12-slot/10-pole FSCW-PM machine and vibration experiment platform. The experimental results of the three-phase no-load back-EMF waveforms at the speed of 310 r/min are shown in Fig. 17(a). The experimental and simulated results of the



**Fig. 15.** (Color online) Modal experiment of prototype.

**Table 4.** (Color online) Modal shape and frequency.

Order	2nd	
Modal shape		
Modal frequency	FEM	2125Hz
	Measured	2109Hz
	Error	0.8%

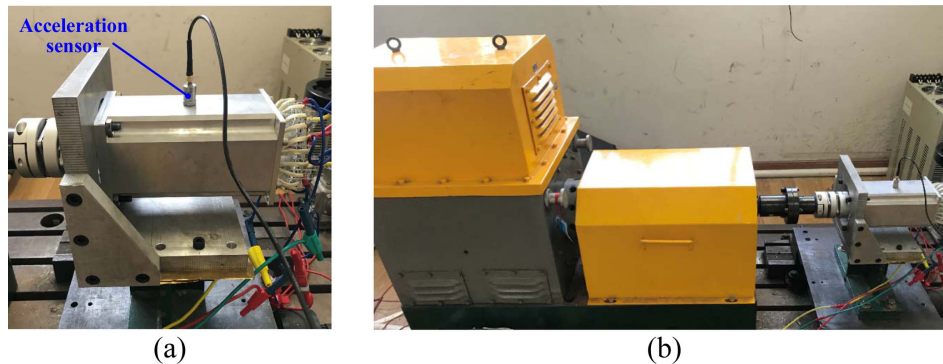


**Fig. 16.** (Color online) Vibration experiment. (a) Prototype. (b) Experiment platform.

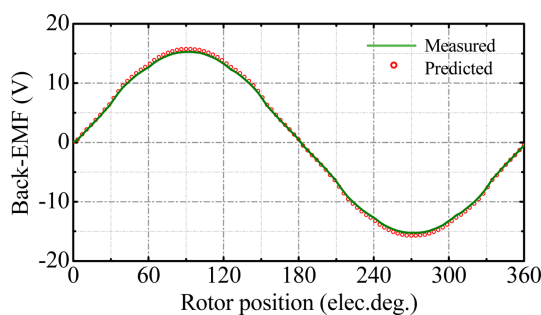


**Fig. 17.** (Color online) Phase back-EMF. (a) Experimental results (10 V/div, 10 ms/div). (b) Comparison of the experimental and simulated waveforms.

back-EMF waveforms are compared in Fig. 17(b). It can be seen that the measured result is about 3 % lower than the simulated one, which is mainly due to the effect of lamination factor and manufacturing error.

The acceleration sensor is fixed to the surface of the machine housing to collect vibration data. Fig. 18 exhibits the comparison of vibration acceleration between the predicted and measured results at rated-load. The peak amplitude of vibration acceleration is occurred at frequency  $2f_0$ , and the predicted results match with that of the experimental ones. It should be pointed out that since the machine is tightly fixed on experiment platform, it is in a constrained state, rather than a free state. Consequently, the 2<sup>nd</sup> modal frequency advances to about 1125 Hz, but the resonance still does not happen. Fig. 19 compares the vibration acceleration of the 12-slot/10-pole prototype machine under no-load and load conditions. The acceleration amplitude at rated-load is much larger than the one at no-load condition. It illustrates that the lowest order radial force is mainly result from the armature MMF harmonic, the newly designed machine can effectively reduce armature MMF tooth harmonics, and thus reducing electromagnetic vibration, which will be verified in Section 6.3.

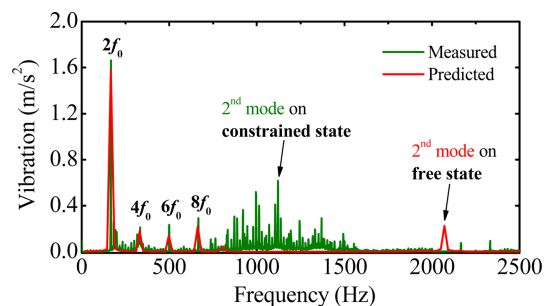


**Fig. 18.** (Color online) Comparison of measured and predicted vibration results.

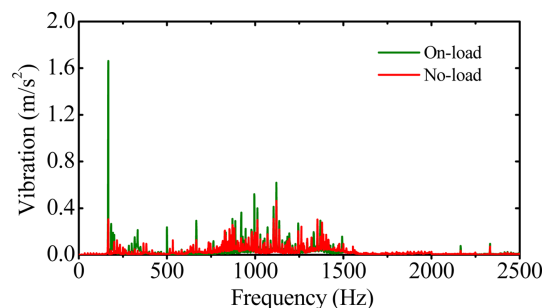


**Fig. 19.** (Color online) Comparison of vibration under on-load and no-load conditions.

### 6.3. Reduction Verification of Electromagnetic Vibration

Based on the foregoing analysis on radial force, the newly designed FSCW-PM machine has greatly reduced the 2<sup>nd</sup> order radial force harmonics. Fig. 20 compares the vibration deformation between the existing and proposed machines at 167 Hz. Because the 2<sup>nd</sup> order radial force harmonics play the dominant role, the vibration shapes are ellipse. Due to the reduction of 2<sup>nd</sup> radial force harmonics, the vibration displacement of the newly designed machine reduced from 1.8  $\mu\text{m}$  to 0.33  $\mu\text{m}$ . Fig. 21 compares the electromagnetic vibration acceleration of the existing and proposed 12-slot/10-pole FSCW-PM machines

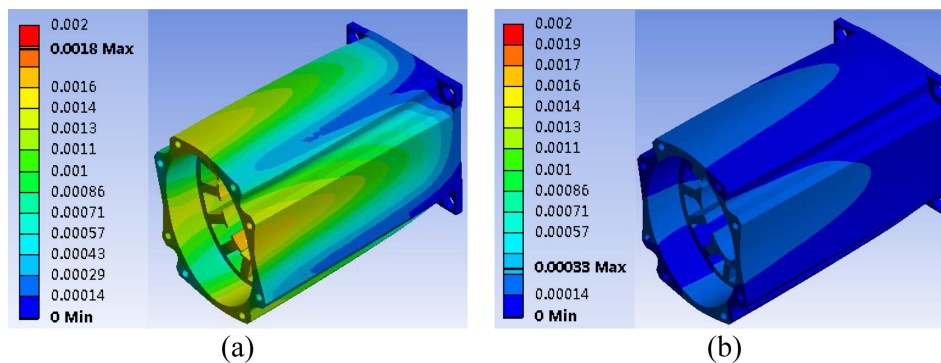


**Fig. 20.** (Color online) Vibration deformation of stator core. (a) Existing. (b) Proposed.

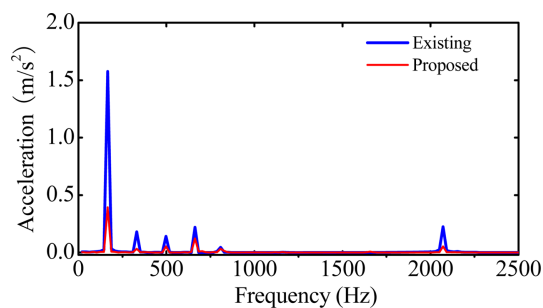


**Fig. 21.** (Color online) Vibration acceleration comparison of existing and proposed machines.

in frequency range of 10 to 2500 Hz. The maximum value of electromagnetic vibration occurs at  $2f_0$  (166.7 Hz), which is consistent with the previous analysis of radial force. The electromagnetic vibration of the 12-slot/10-pole FSCW-PM machine had been effectively reduced by adopting the newly design stator structure. So, the new stator structure has great significance for reducing the electromagnetic vibration of the 12-slot/10-pole FSCW-PM machine.

## 7. Conclusion

In this paper, the unequal teeth design for vibration reduction of FSCW-PM machines has been designed and analyzed. This paper begins with the analysis of the lowest order radial force harmonic generation mechanism of FSCW-PM machines. Through the calculation of the lowest order radial force of 12-slot/10-pole machine, it has been found that the armature MMF tooth harmonic contribute most to the lowest order radial force. Then, a new stator structure has been designed to reduce armature MMF tooth harmonic by adopting unequal teeth technique. The tooth harmonic and 2<sup>nd</sup> order radial force have been reduced 43.4 % and 43.2 %, respectively, while the output torque is kept almost invariable. Subsequently, the modal analysis and experiment has been conducted to obtain

modal parameters such as modal shapes and frequencies. The frequencies of radial force harmonics are far from the corresponding modal frequencies, so the resonance has been avoided. Finally, the vibration simulation and experiment have been conducted on the prototype. Both results have verified the correctness of radial force derivation, and it shows that the newly designed machine effectively reduce the electromagnetic vibration. The analyses of this paper for vibration reduction by unequal tooth technique is also useful for other FSCW-PM machines.

## Acknowledgment

This work was supported by National Natural Science Foundation of China (Projects 51977099 and 51777090), by Natural Science Foundation of Jiangsu Province (Project BK20171298), by Key Research and Development Program of Jiangsu Province (Project BE2018107), and by the Priority Academic Program Development of Jiangsu Higher Education Institutions.

## References

- [1] Y. Wang, R. Qu, and J. Li, *IEEE Trans. Ind. Appl.* **51**, 2208 (2015).
- [2] L. J. Wu and Z. Q. Zhu, *IEEE Trans. Ind. Electron.* **61**, 4990 (2014).
- [3] G. Choi and M. Jahns, *IEEE Trans. Magn.* **52**, 8105904 (2016).
- [4] G. Valente, L. Papini, A. Formentini, C. Gerada, and P. Zanchetta. *IEEE Trans. Ind. Electron.* **65**, 5395 (2018).
- [5] M. S. Islam, R. Islam, and T. Sebastian, *IEEE Trans. Ind. Appl.* **50**, 3214 (2014).
- [6] E. Carraro, N. Bianchi, S. Zhang, and M. Koch, *IEEE Trans. Ind. Appl.* **54**, 2276 (2018).
- [7] Y. Mao, G. Liu, and H. Zhou, *J. Magn.* **22**, 579 (2017).
- [8] F. Lin, S. Zuo, W. Deng, and S. Wu, *IEEE Trans. Ind. Electron.* **65**, 4524 (2018).
- [9] D. Fodorean, M. Sarrazin, C. Martis, J. Anthonis, and H.

- Auwerker, IEEE Trans. Ind. Electron. **52**, 2892 (2016).
- [10] F. Lin, S. Zuo, and X. Wu, IET Electr. Power Appl. **10**, 900 (2016).
- [11] N. Tang and I. P. Bron, IEEE Trans. Magn. **54**, 5 (2018).
- [12] G. Dajaku, H. Hofmann, F. Hetemi, X. Dajaku, W. Xie, and D. Gerling, IEEE Trans. Ind. Electron. **63**, 4137 (2016).
- [13] M. V. Cistelecan, F. Ferreira, and M. Popescu, IEEE Trans. Energy Convers. **25**, 348 (2010).
- [14] V. I. Patel, J. Wang, W. Wang, and X. Chen, IEEE Trans. Ind. Appl. **50**, 2554 (2014).
- [15] W. Zhao, J. Zheng, J. Ji, S. Zhu, and M. Kang, IEEE Trans. Ind. Electron. **65**, 9266 (2018).
- [16] J. Ma and Z. Q. Zhu, 2017 IEEE International Electric Machines and Drives Conference (IEMDC), 1 (2017).
- [17] Y. Mao, G. Liu, W. Zhao, J. Ji, and Z. Wang, IET Electr. Power Appl. **12**, 747 (2018).
- [18] S. Zuo, F. Lin, and X. Wu, IEEE Trans. Ind. Electron. **62**, 6204 (2015).
- [19] M. Wu, W. Zhao, J. Ji, J. Zheng, and J. Luo, J. Magn. **23**, 218 (2018).
- [20] R. Islam and I. Husain, IEEE Trans. Ind. Appl. **46**, 2346 (2010).
- [21] G. He, Z. Huang, R. Qin, and D. Chen, IEEE Trans. Magn. **48**, 1924 (2012).